Room-Temperature Methane Oxidation to Formaldehyde Mediated by $CoMoO^+$ Gas-Phase Cations

Lei-Ting Zhang,[a] Chu-Man Sun,[a] Li-Li Xing,*[b] Donald G. Truhlar,*[c] Feng-Xiang Zhang,[a] Lian-Rui Hu,[d] Jia-Bi Ma*[a]

[a] Lei-Ting Zhang, Chu-Man Sun, Feng-Xiang Zhang, Jia-Bi Ma
Department Key Laboratory of Cluster Science of Ministry of Education, Beijing Key Laboratory of Photoelectronic/Electrophotonic Conversion Materials, School of Chemistry and Chemical Engineering
Beijing Institute of Technology
Beijing 102488, China

[b] Li-Li Xing
Energy and Power Engineering Institute
Henan University of Science and Technology
Luoyang, Henan 471003, China

[c] Donald G. Truhlar
Department of Chemistry, Chemical Theory Center, and Minnesota Supercomputing Institute
University of Minnesota
Minneapolis, Minnesota 55455-0431, United States

[d] Lian-Rui Hu
Shanghai Key Laboratory of Green Chemistry and Chemical Processes, Shanghai Frontiers Science Center of Molecule Intelligent Syntheses, School of Chemistry and Molecular Engineering
East China Normal University
Shanghai, 200062, China

methane, formaldehyde, transition metal, gas phase

ABSTRACT: Formaldehyde (HCHO) is a fundamental chemical feedstock with widespread industrial applications. The direct oxidation of methane by oxygen to formaldehyde ($CH_4 + 1/2O_2 \rightarrow H_2 + HCHO$) under mild conditions represents an attractive but challenging transformation, as it requires both activation of the inert C–H bonds of CH_4 and suppression of overoxidation to products such as carbon dioxide. In this work, mass spectrometry experiments combined with theoretical calculations reveal that $CoMoO^+$ cations can efficiently mediate this transformation at room temperature. The unique electronic structure of $CoMoO^+$ facilitates the formation of a crucial $CoMoOCH_2^+$ intermediate during the reaction with CH_4 and prevents methanol formation. In the subsequent oxidation reaction, the Mo atom in $CoMoO^+$ serves as the active site for O_2 adsorption, and both Mo and Co atoms act as electron donors to activate O_2, leading to the formation of the C–O bond in formaldehyde. This work reports the first gas-phase example of achieving conversion of CH_4 to HCHO and its radical derivatives by O_2 at room temperature using heteronuclear non-noble metal cations. Remarkably, the $CoMoOCH_2^+$ cation maintains high reactivity after adsorbing one or two CH_4 molecules. These findings provide new mechanistic insights into selective methane activation and conversion.

1. INTRODUCTION

Formaldehyde (HCHO) is a fundamental C1 building block and is widely used in industrial applications, including the production of resins, plastics, and various fine chemicals.[1] Among C1 molecules (CO_2, CO, HCOOH, CH_4, etc.), HCHO is a highly reactive substrate, making it particularly valuable for synthesis of chiral products.[2] Currently, industrial HCHO manufacturing relies on energy-intensive methanol oxidation–dehydrogenation (> 500 °C), catalyzed by silver or metal oxides, consuming 35% of global methanol output and generating substantial CO_2 emissions.[3]

Methane (CH_4), the primary component of natural gas, represents a promising yet underexploited feedstock for direct HCHO production.[4,5] However, this transformation faces two fundamental challenges:

- CH_4 is relatively inert due to its high C–H bond energy of 4.5 eV and its high HOMO-LUMO gap of 11 eV, and this typically necessitates harsh reaction conditions or multi-step processes.[6]
- In conventional CH_4 oxidation processes, HCHO is a transient intermediate ($CH_4 \rightarrow CH_3OOH \rightarrow CH_3OH \rightarrow HCHO \rightarrow CO_x$), [7] and is prone to over-oxidation to CO_2.

However, selectively oxidizing CH_4 with O_2 to form HCHO as a final product remains particularly challenging because of this high reactivity.

Because of the abundance of methane resources and the industrial significance of oxygenate products, the conversion of CH_4 into value-added oxygenates represents a highly promising yet challenging frontier in heterogeneous catalysis.[8,9] Catalytic systems that employ O_2 as a thermal oxidant such as Fe_2/SiO_2[10] and B_2O_3-based catalysts.[11] typically require high temperatures (> 800 K). In contrast, low-temperature (< 493 K) conversions rely on strong oxidants such as H_2O_2[12] or noble metal active sites.[13] Although photocatalysis has shown remarkable selectivity, such as 96.5% selective for CH_4-to-HCHO conversion via synergistic Cu single atoms and $W^{\delta+}$ on oxygen-vacancy-rich WO_3,[14] and 71.2% selectivity with Ag_1-ZnO at ambient pressure,[15] the efficient and selective oxidation of methane to formaldehyde with O_2 under mild conditions remains a major challenge.

Previous studies have reported that isolated MoO_x species supported on SiO_2[16], ZrO_2[17], and SiC[18] can catalyze the partial oxidation of CH_4. These systems typically employ N_2O or O_2 as oxidants at elevated temperatures (>573 K), where Mo serves as the active site for methane partial oxidation. In addition, bimetallic catalysts have attracted increasing attention in recent years. For instance, Cu–MoO_x bimetallic catalysts exhibit enhanced performance via transition-metal synergy, achieving high yield of HCHO.[19] However, these reported systems face some critical limitations: (1) the requirement of harsh reaction conditions, and (2) the production of mixed oxygenates (e.g., HCHO, CH_3OH, and CO_2) due to over-/under-oxidation. These issues complicate product separation and diminish overall efficiency. Therefore, it is desirable to develop strategies for designing active sites in heterogeneous catalysts to realize high selectivity of HCHO under mild conditions.[20,21]

Combined with theoretical methods, gas-phase experiments on isolated reactants provide an ideal field for revealing mechanistic insights of crucial factors affecting the reactivity of active sites at a molecular level.[22-34] Dehydrogenation of methane to generate $[M]CH_2$ mediated by 5d metal cations has been very well studied,[35-40] and the reactivity of these metal-carbene ions has been further investigated.[41] Since the methane conversion to formaldehyde at room temperature is challenging, only a limited number of studies have investigated the reactivity of metal oxide clusters for CH_4-to-HCHO conversion, including $Al_2O_3^+$, ReO_4^+, $AuNbO_3^+$, $NiAlO_3^+$, $AuV_2O_6^+$, $RhVO_3^-$, $AuTi_3O_8^-$, and $PtAl_2O_4^-$.[42-49] There are three types of reaction mechanisms:

- Oxygen radical ($O^{\bullet-}$) mediated hydrogen atom transfer (HAT).[42-45]
- Lewis acid-base-pair activation.[46]
- Noble-metal-centered pathways.[47-49]

These mechanisms involve cluster-bound oxygen rather than molecular O_2 as oxygen sources. To our knowledge, there is no such gas-phase example that can efficiently convert CH_4 to HCHO using O_2. Since O_2 is the most abundant oxygen source on Earth, it is desirable to synthesize active sites which can achieve this process, especially if it can be done at room temperature.

In the work reported here, we present an efficient and promising approach for formaldehyde synthesis ($CH_4 + 1/2O_2 \rightarrow H_2 + HCHO$) mediated by $CoMoO^+$ cations at room temperature. A homemade time-of-flight mass spectrometer (TOF-MS) was used to examine the gas-phase reactions. The reaction proceeds via two steps:

- CH_4 dehydrogenation: $CoMoO^+$ cations enable the dehydrogenation of CH_4, yielding $CoMoOCH_2^+$ and H_2.
- Oxygen insertion: $CoMoOCH_2^+$ reacts with O_2, generating HCHO or $HCO^\bullet$ radicals.

Similar reaction channels can also be observed after $CoMoOCH_2^+$ associates with one or two CH_4 molecules, and the reaction rates do not slow down once more CH_4 molecules are attached. Typically, gas-phase ions either react with adsorbed CH_4 molecules or lose reactivity through CH_4 adsorption. However, the observed behavior of $CoMoOCH_2^+$ constitutes an exception, and it closely mimics the multi-molecule binding environment characteristic of practical catalytic systems.

2. METHODS

2.1. Experimental methods. We used a homemade time-of-flight mass spectrometer (TOF-MS) coupled with a linear ion trap (LIT) reactor to examine the gas-phase reactions. Because the experiment details have been described in previous works,[50,51] only a brief description is given here. The ions of interest were generated by laser ablation of a rotating and translating ^{98}Mo/Co disk target (1:1 molar ratio of ^{98}Mo:Co) in the presence of 0.5‰ O_2 seeded in a He carrier gas at a backing pressure of 3 atm. The ^{98}Mo metal powder (98.61% isotopic purity) was purchased from ISOFLEX (San Francisco, California, USA), and the cobalt metal powder (99.9% purity) was obtained from Macklin (Shanghai, China). We used a 532 nm (second harmonic of Nd^{3+}: yttrium aluminum garnet–YAG) laser with an energy of 5–8 mJ/pulse and a repetition rate of 10 Hz. The $CoMoO^+$ cations were then mass-selected by a quadrupole mass filter (QMF) and entered a LIT reactor, where they reacted first with CH_4 and then with O_2. In previous studies, it has been shown that the ions are thermalized to (or close to) room temperature before reacting.[52] The ions ejected from the LIT were detected by the reflectron TOF-MS.

2.2. Theoretical methods. To study the reaction mechanism of the $CoMoO^+/CH_4/O_2$ system, density functional theory (DFT) calculations were performed using the *Gaussian 16* program package.[53] To decide which functional to use for these studies, we compared bond enthalpies from several density functionals to relevant experimental bond energies.[54] The bond enthalpies are for 0 K, at which temperature they equal the change in potential energy upon bond breaking plus the change in zero point energy. Table S1 shows that, out of 19 functionals tested, MN15-L[55] performed best (figures and tables with a prefix S are in Supporting Information). Therefore, we adopted the MN15-L exchange-correlation functional for studying the mechanism. The MN15-L functional gives an overall mean unsigned error (MUE) of 2.32 kcal/mol on the AME422 database for atoms and molecules.[55] For all of the calculations, we used the def2-TZVP basis set[56] for Mo and Co atoms and the cc-pVTZ basis set[57] for C, H, and O atoms. To get the lowest-energy SCF solution for $CoMoO^+$ and $CoMoOCH_2^+$, we used *Gaussian*'s fragment option (fragment=N) for the initial guess of the orbitals. For the

calculations of the reaction mechanism, the geometry of each intermediate (**I**) and transition state (**TS**) was optimized. We confirmed that each intermediate has no imaginary frequency, and each **TS** has one imaginary frequency. We also calculated minimum-energy paths[58-60] (called IRCs in *Gaussian*) to ensure that the **TS**s connect the local minima that are the preceding and following intermediates along the reaction path.

All open-shell calculations are unrestricted Kohn-Sham (UKS) calculations,[61] We performed stability checks for all the structures involved in the reaction pathway, including intermediates and transition states. The calculations indicate that no significant wave function instability is present. All energetic results reported in this paper are reported as enthalpies in eV at 0 K. The 0 K enthalpy is calculated as the sum of the electronic energy (including nuclear repulsion) at the optimized structure and the zero-point vibrational energy (ZPE). Natural bond orbital (NBO) analysis was performed using NBO 6.0,[62] and two-dimensional electron localization functions were obtained using Multiwfn 3.8.[63]

3.RESULTS

3.1. Reactivity. The time-of-flight mass spectra for the reactions of mass-selected $CoMoO^+$ cation with CH_4 and O_2 are given in Figure 1. Panel a shows the reference spectrum with inert He as the reactant gas; $CoMoO_2^+$ is present due to the residual water in the LIT. Upon reaction with 72 mPa CH_4 (panel b), the $CoMoO^+$ signal decreases, concomitant with the emergence of a dominant $CoMoOCH_2^+$ peak, indicating methane dehydrogenation with H_2 elimination, which is reaction 1 in Table 1. To assess the oxygen dependence of reactivity and to fully elucidate the unique reactivity of $CoMoO^+$, we systematically investigated reactions of $CoMo^+$, $CoMoO_2^+$ and $CoMoO_3^+$ with CH_4. As the number of oxygen atoms increases, the reactivity follows the order: $CoMoO^+ > CoMoO_2^+ > CoMoO_3^+ > CoMo^+$. $CoMoO_2^+$ exhibits low dehydrogenation activity, and for $CoMoO_3^+$, the only adsorption product observed is $CoMoO_3CH_4^+$. Without the oxo ligand, no products of adsorption or reaction were observed between $MoCo^+$ and CH_4, as shown in Figure S1.

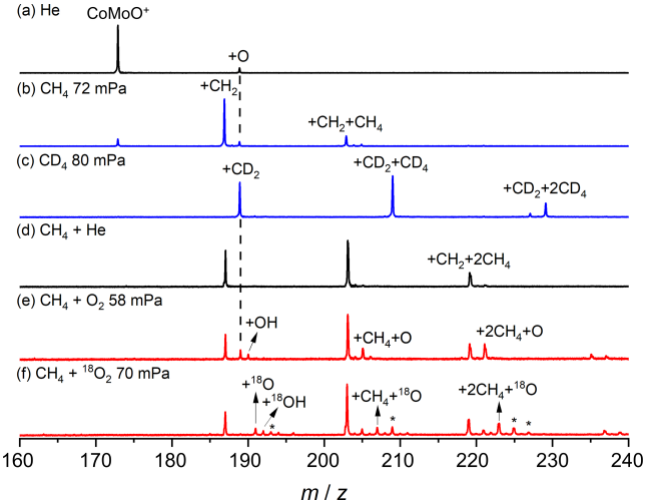

Figure 1. (a–c) Time-of-flight mass spectra after 0.9 ms for the reactions of mass-selected $CoMoO^+$ with (a) He, (b) CH_4, and (c) CD_4. (d–f) Time-of-flight mass spectra after 1 ms for the generated intermediate products $CoMoOCH_2^+$ reactions in the presence of (d) He, (e) O_2, and (f) $^{18}O_2$. The peaks marked with asterisks in panels (f) can be assigned to $CoMo^{18}O_2^+$, $CoMo^{18}O_2^+CH_4$, $CoMo^{18}O_2^+(CH_4)_2$, and $CoMoO^{18}O_3^+CH_4$ due to isotope exchange. The effective reactant gas pressures are shown in panels b and c, and pressures of O_2 are given in panels e and f.

To investigate the subsequent reaction of $CoMoOCH_2^+$ with O_2, we first reacted the $CoMoO^+$ cations with CH_4 in a reactant gas of CH_4 and He (Figure 1d). After most of the $CoMoO^+$ cations were converted to the intermediate product $CoMoOCH_2^+$, we pulsed O_2 molecules into the LIT reactor. When 58 mPa of O_2 molecules were introduced and reacted with the intermediate $CoMoOCH_2^+$ for approximately 1 ms, two primary product peaks appeared; we assigned them as $CoMoO_2^+$ and $CoMoO_2H^+$, which suggests the evaporation of neutral HCHO (and H_2/CO) and $HCO^•$ radicals (Figure 1e; reactions 2a and 2b in Table 1). Isotopic labeling experiments with CD_4 and $^{18}O_2$ (panels c and f of Figure 1) confirm the reaction channels mentioned above. The product distribution in Figure 1f (predominant $CoMoO^{18}O^+$ vs. minor $CoMo^{18}O_2^+$) indicates that O_2 is the major oxygen source for formaldehyde formation. The formation of $CoMoO^{18}O^+CH_4$ and $CoMoO_{18}O^+(CH_4)_2$ verifies the reaction pathways of $CoMoOCH_2^+CH_4$ and $CoMoOCH_2^+(CH_4)_2$ with O_2. Experimental attempts to reduce $CoMoO_2^+$ with CO or H_2 did not lead to the observation of $CoMoO^+$.

The pseudo-first-order reaction rates (k_1) for the reactions of $CoMoO^+$ cations with CH_4 and O_2 from fits to the data in Figure S2 are given in Table 1. We obtain k_1 of $(1.4\pm0.3)\times10^{-10}$ cm^3 $molecule^{-1}$ s^{-1} for CH_4 dehydrogenation, and comparing this to the Langevin model[64,65] for the collision rate gives a reaction efficiency (Φ) of 14%. Similar reaction channels can also be observed after $CoMoOCH_2^+$ adsorbs one or two CH_4 molecules. It is noteworthy that after the reaction of $CoMoOCH_2^+$ with O_2 to form $CoMoO_2^+$, partial CH_4 molecules remain in the ion trap; therefore, $CoMoO_2^+CH_4$ could presumably form from the reaction between $CoMoO_2^+$ and CH_4. However, we conclude that the $CoMoO_2^+CH_4$ is primarily derived from the reaction of $CoMoOCH_2^+(CH_4)$ with O_2 rather than from that of $CoMoO_2^+$ with O_2, based on the following observation: when $CoMoO_2^+$ reacts with CH_4, a substantial amount of $CoMoO_2CH_2^+$ is concurrently generated (Figure S1b2). In contrast, the abundance of this product detected in Figure 1e is remarkably low. From Figure 1f, the reaction rates of $CoMoOCH_2^+$, $CoMoOCH_2^+(CH_4)$, and $CoMoOCH_2^+(CH_4)_2$ with O_2 show a ratio of 1:0.46:0.82, indicating that methane adsorption does not lead to significant rate reduction.

3.2. Structure characterization and reaction mechanisms. The reaction mechanisms of the observed CH_4 oxidation to HCHO by O_2 mediated by $CoMoO^+$ were elucidated by DFT calculations. Figure S3 shows a number of stationary structures discovered for $CoMoO^+$, $CoMoOCH_2^+$, and $CoMoO_2^+$. For example, the figure shows that the lowest energy structure of $CoMoO_2^+$ is a chain Co–O–Mo–O^+ rather than a cycle. We calculated even more structures, such as Mo–O–Co–O^+, but they were higher in energy than the ones illustrated.

Figures 2 and 3 show the reaction mechanisms and lowest-energy structures for the formation of HCHO and $HCO^•$ by $CoMoO^+$. DFT calculations indicate that the lowest-energy structure of $CoMoO^+$ possesses a Mo–Co bond and has a quintet spin multiplicity. We found that as one moves

along the reaction path, only triplet states are low enough in energy to be accessible, so the reaction might involve two-state reactivity (TSR), which has been observed in several other reactions involving transition metals.[66-70] In TSR, there are two paths from reactants to products; the first is an electronically adiabatic path on a single potential energy surface described within the Born–Oppenheimer (BO) approximation, and the second involves one or more transitions between potential energy surfaces corresponding to different spin multiplicities.

Table 1. Reactions, branching ratios, rate constants, and reaction efficiencies.

	Reactions	BP[a]	k_1[b]/(cm^3 molecule^{-1} s^{-1})	Φ[c]
(1)	$CoMoO^+ + CH_4 \rightarrow CoMoOCH_2^+ + H_2$	100%[d]	$(1.4\pm0.3)\times10^{-10}$	14%
(2a)	$CoMoOCH_2^+ + O_2 \rightarrow CoMoO_2^+ + HCHO/H_2 + CO$	68%	$(9.3\pm1.9)\times10^{-11}$	16%
(2b)	$\rightarrow CoMoO_2H^+ + HCO^\bullet$	32%		

[a] BP is the normalized branching percentage of the indicated product.

[b] The rate constants k_1 are from experiments with varying reactant-gas pressure as shown in Figure S2.

[c] $\Phi = k_1/k_{Langevin}$, where $k_{Langevin}$ is a theoretical collision rate.

[d] The 100% branching ratio indicates that the reaction of $CoMoO^+$ with methane only produced $CoMoOCH_2^+$ with no by-products.

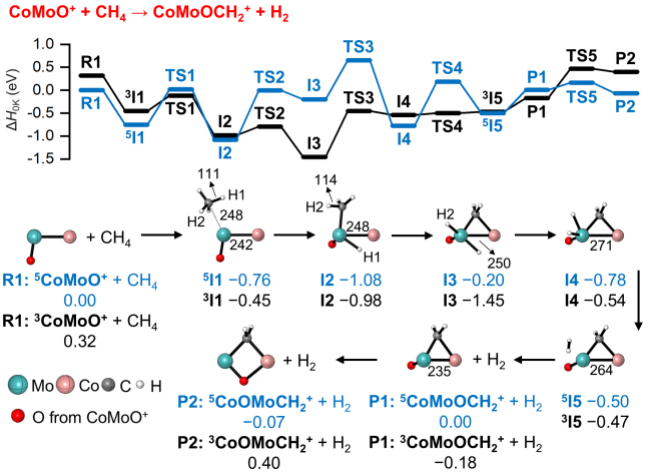

Figure 2. Calculated energy profiles the reaction of $CoMoO^+$ with CH_4 to generate $CoMoOCH_2^+$ (two isomers). For each structure, the figure gives bond lengths (in pm) and relative enthalpies ΔH_{0K} (in eV) of intermediates, transition states, and products relative to reactants. The blue and black lines represent the quintet and triplet states, respectively. The transition states are given in Figure S4.

Figure 2 shows that CH_4 is initially adsorbed at the Mo site, which is thermodynamically more favorable than being adsorbed on the Co atom by 0.15 eV. The isomerization of methane from the Co to the Mo adsorption site proceeds via a low energy barrier of 0.37 eV (Figure S5). A possible reaction step where the system might cross to the triplet surface is the first C–H bond activation ^{5}**I1** → ^{3}**TS1**. If the system is to remain on the quintet ground-state surface, it would face insurmountably high transition states (e.g. ^{5}**TS2**, ^{5}**TS3** or ^{5}**TS4**). However, a thermal process becomes feasible through the spin-flip to the triplet spin state. Subsequent activation of the second C–H bond forms a Co–CH_2–Mo triangular unit (^{3}**I2** → ^{3}**I3**). After passing through intermediate ^{3}**I4**, the H1 and H2 atoms combine to form an H_2 molecule (^{3}**I3** → ^{3}**I5**). Then the H_2 unit desorbs from the Mo atom (^{3}**I5** → **P1**), leading to the generation of the triplet $CoMoOCH_2^+$ cation.

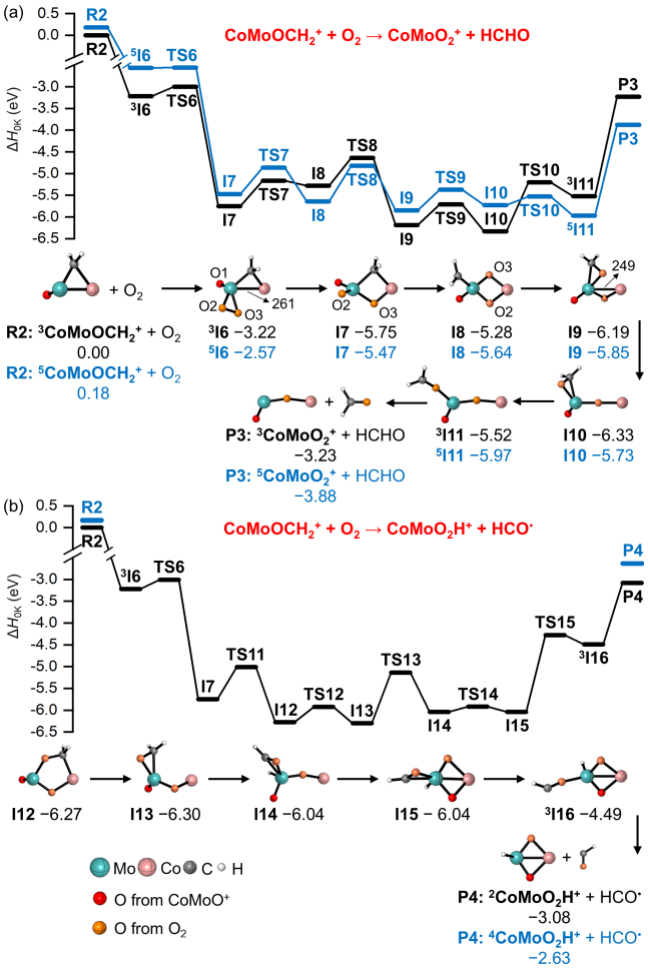

Figure 3. Calculated energy profiles for the reaction of $CoMoOCH_2^+$ with O_2 to generate (a)HCHO and (b)HCO•. For each structure, the figure gives bond lengths (in pm) and relative enthalpies ΔH_{0K} (in eV) of intermediates, transition states, and products relative to reactants. The blue and black lines represent the quintet and triplet states, respectively. The transition states are given in Figure S4.

Figure 3 shows the reaction profiles for the oxidation of $CoMoOCH_2^+$ by O_2 to form HCHO and HCO•. In Figure 3a, the incoming O_2 is attached to the Mo atom in an η^2 coordination mode to form intermediate ^{3}**I6** with a binding energy of −3.22 eV. Subsequently, ^{3}**I6** overcomes a barrier (^{3}**TS6**) to cleave the O–O bond by cooperation between Mo and Co, yielding the more stable ^{3}**I7**. In ^{5}**I8**, the O atoms bridge the

Mo and Co atoms in a quintet state, followed by the breaking of the Co–O bond, after which the triplet is again lower in energy (^{5}**I8** → ^{3}**I9**). Then the C–O coupling occurs in the step of ^{3}**I9** → ^{3}**I10**. Finally, after another possible TSR step, HCHO desorbs from the Mo atom (^{5}**I11** → **P3**), resulting in the generation of the $CoMoO_2^+$ cation in the quintet spin state. In this reaction pathway, the O1 atom from $CoMoO^+$ can also serve as the oxygen source for the formation of HCHO, but this pathway is thermodynamically less favorable compared to the route using oxygen atoms from O_2. This computational finding is consistent with isotopic mass spectrometry results. Figure S6 in SI shows an alternative reaction pathway from $CoMoOCH_2^+/O_2$, generating HCHO and another low-lying isomer of $CoMoO_2^+$ that features two bridging oxygen atoms.

We also evaluated the possibility of generating H_2/CO from the reaction of $CoMoOCH_2^+$ with O_2 (Figure S7). This pathway is found to be accessible. The formation of H_2/CO requires the cleavage of all four C–H bonds in CH_4. Calculations based Rice–Ramsperger–Kassel–Marcus (RRKM) theory[71] and RRKM-based variational transition state theory (VTST)[72] indicate that the rate-determining step for the HCHO generation pathway is kinetically and thermodynamically comparable to that of the H_2/CO pathway (Table S2, SI). Therefore, HCHO and H_2/CO may be formed as co-products. The calculated rate constants for the rate-determining steps of HCHO and H2/CO formation pathways in Table S2 indicate that the rate constants for HCHO formation proceeds approximately ten times faster than that of H_2/CO formation. Given the overall 68% branching ratio for these combined channels (excluding the 32% formaldehyde radical channel), the relative rate constants yield a calculated distribution of approximately 34% for HCHO and 34% for H_2/CO. Consequently, HCHO formation (including 32% formaldehyde radical) is the dominant pathway, with a selectivity exceeding 60%.

The lowest-energy isomer of $CoMoOCH_2^+$ features a terminal oxygen atom bonded to Mo. An alternative isomer ($CoOMoCH_2^+$ in Figure 3) in which the oxygen bridges Mo and Co have only a slightly higher energy (+0.11 eV). Therefore, reactions starting with $CoOMoCH_2^+$ were also considered, but we found that the formation of $CoOMoCH_2^+$ requires overcoming the barrier above zero (with respect to the separated reactants), so it is not favorable (Figure 2).

The pathway to form HCO• is shown in Figure 3b. Up to intermediate ^{3}**I7**, this reaction pathway is the same as in Figure 3a. Starting from ^{3}**I7**, a bridging oxygen atom bound Mo undergoes C–O coupling with a carbon atom, forming a five-membered Mo–O–C–Co–O ring. Subsequently, cleavage of the Co–C bond (^{3}**I12** → ^{3}**I13**) is followed by the Mo-mediated activation of the third C–H bond of methane, forming a Mo–H bond (^{3}**I13** → ^{3}**I14**). Thereafter, the Mo–C bond cleavage in ^{3}**I15** produces an HCO• unit. Finally, release of HCO• from ^{3}**I16** yields the ionic product $CoMoO_2H^+$.

4. DISCUSSION

In this study, we report the conversion of CH_4 and O_2 to HCHO mediated by $CoMoO^+$ cations at room temperature ($CH_4 + 1/2O_2 \rightarrow H_2 + HCHO$). The $CoMoO^+$ cations first activate CH_4 to generate H_2 and the crucial intermediate product $CoMoOCH_2^+$. Then, $CoMoOCH_2^+$ reacts with O_2 to produce HCHO and HCO•. While previous reports have identified Pt^+ and $Ta_{1,4}^+$ cations can mediate this transformation,[73-75] our system exhibits superior performance. In particular, Pt^+ shows limited HCHO selectivity (30%); $Ta_{1,4}^+$ cations exhibit moderate HCHO selectivity (35% and 53%, respectively), but more byproducts including CH, CH_2, H_2, and O are also produced. Our work represents the first experimental verification of HCHO (HCO•) production from the oxidation of CH_4 by O_2 mediated by heteronuclear non-noble metal cations.

Mechanistic investigations reveal the critical dependence on reaction sequence: $CoMoO^+$ can firstly react with O_2 to produce $CoMoO_{2\text{-}3}^+$, while there is no sign of HCHO generation through the reaction of $CoMoO_{2\text{-}3}^+$ with CH_4 (Figure S1). Therefore, the formation of the metal-methylidene intermediate (M^+–CH_2) is a key requirement for methane dehydrogenation ($CH_4 \rightarrow CH_2 + H_2$). We point to three underlying features contributing to the capability of this intermediate for methane oxidation:

- Neither Mo^+ nor Co^+ can form the CH_2 unit in reactions with CH_4 since the Mo^+–CH_2 and Co^+–CH_2 bond energies are not large enough.[76] However, the $CoMoO^+$ cation achieves the necessary binding energy ($CoMoO^+$–CH_2: 4.67 eV) by synergistic effects: 1) The synergistic effect between Mo and Co atoms enhances CH_2 bonding ($CoMo^+$–CH_2: 4.53 eV > Mo^+–CH_2: 3.06 eV or Co^+–CH_2: 3.48eV). In addition, the presence of the oxo ligand further stabilizes $CoMoO^+$–CH_2, pushing its bond strength (4.67 eV) above the thermodynamic threshold for methane dehydrogenation. It is noteworthy that, although the calculated bond dissociation energy (BDE) of $CoMoO^+$–CH_2 (4.67 eV) is slightly lower than the CH_2–H_2 bond energy (4.74 eV at 0 K) reported in the current Active Thermochemical Tables,[77] the value lies within a reasonable error margin of ±0.1 eV.
- Electronic structure analysis shows that the Mo and Co sites of $CoMoO^+$ are positively charged, with electron configurations $4d^{4.33}5s^{0.71}$ on Mo and $3d^{7.79}4s^{0.71}$ on Co, as compared to the electron configurations of the neutral atoms: $4d^5 5s^1$ for Mo and $3d^7 4s^2$ for Co. The positive charges on both metal atoms enhance the electrophilicity of complex, facilitating electron acceptance from the CH_2 unit.
- The LUMO levels of $CoMoO^+$ cations are more closely aligned (favoring catalysis[78]) with the HOMO level of CH_2 than are the LUMO levels of Co^+, Mo^+, or $CoMo^+$. This is illustrated by DFT calculations presented in Figure 4.

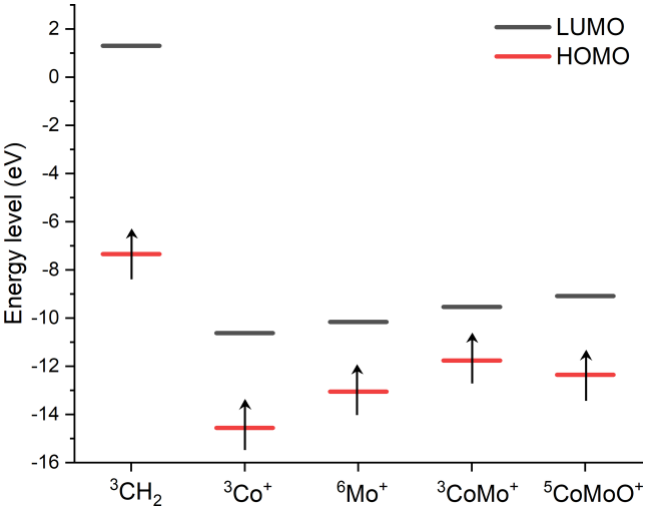

Figure 4. HOMO and LUMO orbital energies of CH_2, Co^+, Mo^+,

$CoMo^+$ and $CoMoO^+$. The ground states of CH_2, Co^+, Mo^+, $CoMo^+$, and $CoMoO^+$ are respectively triplet, triplet, sextet, triplet, and quintet, with the HOMO orbitals all singly occupied.

To further understand the charge flow during catalysis, we calculated natural charges along the reaction paths of Figures 2 and 3a and analyzed them in terms of three stages: CH_4 dehydrogenation, O_2 activation, and HCHO formation; see Figure 5a. In the initial CH_4 dehydrogenation region (^{5}**I1** → **P1**), Mo and Co atoms act cooperatively, with Mo donating 0.14 *e* and Co donating 0.34 *e* to activate CH_4 (^{5}**I1** → ^{3}**I3**). During this process, the charge of the C atom varies slightly. The subsequent O_2 activation stage ($CoMoOCH_2^+ + O_2$ → ^{5}**I8**) features pronounced electron transfer from the Mo and Co centers to O2 and O3 atoms, driving the O–O bond cleavage. In Figure 5b, the two-dimensional electron localization function (ELF) analysis of ^{5}**I8** is conducted, which confirms the critical electron-donor role of the $CoMoO^+$ system in oxygen activation. During the final HCHO formation stage (^{5}**I8** → **P3**), the C atom undergoes substantial electron depletion, continuously donating 0.82 *e* to the Co and O3 atoms, and thus the charge on the C atom changes from negative to positive value in the whole process. The ELF analysis of ^{5}**I8** reveals that electrons are predominantly localized in the Mo–O and Mo–C bonds. The high spin density on the C atom suggests that the O2 atom can accept electrons from C, thereby promoting the C–O bond formation (^{5}**I8** → ^{3}**I9**). Throughout the reaction, the Mo and Co atoms serve as efficient electron reservoirs, driving the oxidation of CH_4 by O_2. Initially, they activate the C–H bond to generate the intermediate product $CoMoOCH_2^+$, and then they break the O–O bond, which steers the reaction along the kinetically favorable pathway toward HCHO production.

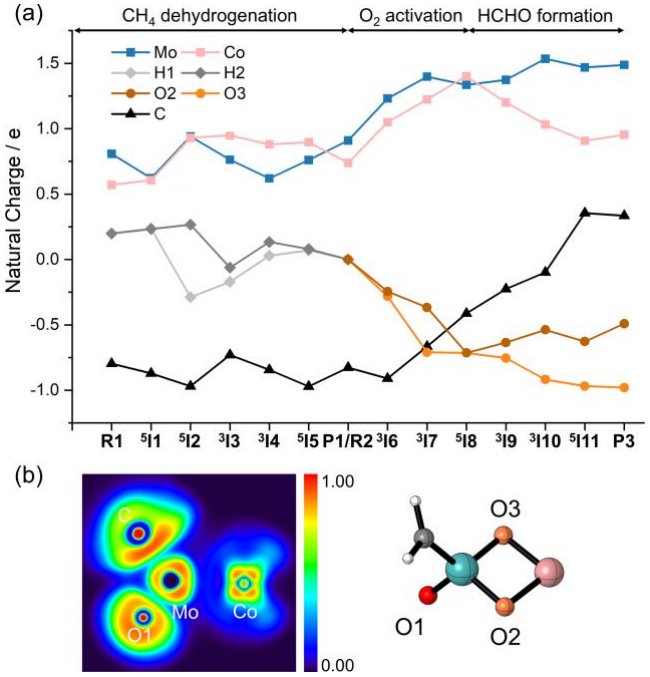

Figure 5. (a) Charges on atoms of stationary points along reaction coordinates of $CoMoO^+$ with CH_4 and O_2. The charge of O1 remains essentially constant throughout and is omitted for clarity. (b) The two-dimensional electron localization function (ELF) of ^{5}**I8**, where a high ELF value means that electrons are greatly localized.

We find that $CoMoOCH_2^+$ maintains its reactivity toward O_2 for HCHO formation even when pre-coordinated with one or two CH_4 molecules, and this phenomenon is rarely reported in the gas-phase studies. To understand this exceptional reactivity, we investigated the reaction profile for $CoMoOCH_2^+(CH_4)_2$ and found that it is very similar to that for $CoMoOCH_2^+$. The association energy of CH_4 at Mo and Co sites is similar in $CoMoO^+$, $CoMoOCH_2^+$ and $CoMoOCH_2^+(CH_4)$, ranging from −0.6 eV to −0.9 eV (see Table S3), which is beneficial for the migration of methane and prevents the desorption of methane in subsequent reactions. RRKM and VTST calculations indicate that the decomposition of oxygen on the intermediates is faster than that of the desorption of CH_4. Plots similar to Figure 5a but for the reaction coordinates of $CoMoOCH_2^+$ and $CoMoOCH_2^+(CH_4)_2$ are given in Figure S8. For $CoMoOCH_2^+(CH_4)_2$, CH_4 will migrate from Mo site to Co site when oxygen is added, which enables the Mo site to be exposed, facilitating the capture and activation of oxygen.

5. CONCLUSIONS

In summary, this combined experimental and theoretical study reveals the first heteronuclear non-noble metal cations that mediates the oxidative conversion of CH_4 to HCHO and its radical derivatives by utilizing O_2 as the oxygen source under mild conditions. We have identified the reaction mechanisms of $CoMoO^+$ with CH_4 and O_2. The distinctive electronic structure of $CoMoO^+$ plays an important role in driving a dehydrogenation reaction of methane, leading to the formation of a thermodynamically stable $CoMoOCH_2^+$ intermediate. The Co–CH_2–Mo unit in $CoMoOCH_2^+$ is crucial as the newly formed CH_2 moiety is anchored on the active site. This key intermediate effectively inhibits the formation of methanol, a common product in methane oxidation reactions. The synergistic effect between Mo and Co atoms in $CoMoO^+$ drives the reaction through two critical steps:

- C–H bond activation in CH_4, forming the important intermediate $CoMoOCH_2^+$.
- Subsequently, through the collaborative action of Mo and Co atoms, the O–O bond in O_2 is cleaved and one C–O bond is successfully formed, facilitating the generation of the final product formaldehyde or $HCO^•$.

Remarkably, $CoMoOCH_2^+$ maintains reactivity toward O_2 even after adsorbing one or two CH_4 molecules, closely mimicking the multi-molecule binding scenario in practical catalysis. These findings not only deepen the mechanistic understanding of methane oxidation by bimetallic oxides but also establish a framework for designing efficient bimetallic active sites, which may contribute to the development of efficient and selective catalytic systems in methane conversion.[to be filled in]

ASSOCIATED CONTENT

Supporting Information

The Supporting Information is available free of charge at https://pubs.acs.org/doi/10.1021/jacs[to be filled in]

Additional experimental mass spectra, additional density functional calculations, Cartesian coordinates of optimized structures, and additional references.

AUTHOR INFORMATION

Corresponding Authors

Li-Li Xing − *Energy and Power Engineering Institute, Henan University of Science and Technology, Luoyang, Henan 471003, China; E-mail: xingll2018@haust.edu.cn*.

Donald G. Truhlar − *Department of Chemistry, Chemical Theory Center, and Minnesota Supercomputing Institute, University of Minnesota, Minneapolis, Minnesota 55455-0431, United States; E-mail: truhlar@umn.edu.*

Jia-Bi Ma − *Department Key Laboratory of Cluster Science of Ministry of Education, Beijing Key Laboratory of Photoelectronic/Electrophotonic Conversion Materials, School of Chemistry and Chemical Engineering, Beijing Institute of Technology, Beijing 102488, China; E-mail: majiabi@bit.edu.cn*.

Notes

The authors declare no competing financial interest.

ACKNOWLEDGMENTS

This work is supported by the National Natural Science Foundation of China (Nos. 22222301 and 92461313), the Fundamental Research Funds for the Central Universities (2025CX01013), the National Key Research and Development Program of China (2021YFA1601800), and the U. S. Department of Energy under award DE-SC0023383.

REFERENCES

(1) Bahmanpour A. M.; Hoadley A.; Tanksale A. Critical Review and Exergy Analysis of Formaldehyde Production Processes. *Rev. Chem. Eng.* **2014**, *30*, 583-604.

(2) Desmons S.; Fauré R.; Bontemps S. Formaldehyde as a Promising C1 Source: The Instrumental Role of Biocatalysis for Stereocontrolled Reactions. *ACS Catal.* **2019**, *9*, 9575-9588.

(3) Heim L. E.; Konnerth H.; Prechtl M. H. G. Future Perspectives for Formaldehyde: Pathways for Reductive Synthesis and Energy Storage. *Green Chem.* **2017**, *19*, 2347-2355.

(4) Saha D.; Grappe H. A.; Chakraborty A.; Orkoulas G. Postextraction Separation, On-Board Storage, and Catalytic Conversion of Methane in Natural Gas: A Review. *Chem. Rev.* **2016**, *116*, 11436-11499.

(5) Schwach P.; Pan X.; Bao X. Direct Conversion of Methane to Value-Added Chemicals over Heterogeneous Catalysts: Challenges and Prospects. *Chem. Rev.* **2017**, *117,* 8497-8520.

(6) Han P.; Yan R.; Wei Y.; Li L.; Luo J.; Pan Y.; Wang B.; Lin J.; Wan S.; Xiong H.; Wang Y.; Wang S. Mechanistic Insights into Radical-Induced Selective Oxidation of Methane over Nonmetallic Boron Nitride Catalysts. *J. Am. Chem. Soc.* **2023**, *145,* 10564-10575.

(7) Fan Y.; Zhang P.; Lu R.; Jiang Y.; Pan G.; Wang W.; Zhu X.; Wei S.; Han D.; Niu L. Highly Selective Oxidation of Methane to Formaldehyde on Tungsten Trioxide by Lattice Oxygen. *Catal. Commun.* **2021**, *161*, art. no. 106365.

(8) Ravi M.; Ranocchiari M.; van Bokhoven J. A. The Direct Catalytic Oxidation of Methane to Methanol−a Critical Assessment. *Angew. Chem., Int. Ed.* **2017**, *56*, 16464-16483.

(9) Dummer N. F.; Willock D. J.; He Q.; Howard M. J.; Lewis R. J.; Qi G.; Taylor S. H.; Xu J.; Bethell D.; Kiely C. J.; Hutchings G. J. Methane Oxidation to Methanol. *Chem. Rev.* **2022**, *123*, 6359-6411.

(10) Wachi K.; Yabe T.; Suzuki T.; Yonesato K.; Suzuki K. K. Yamaguchi. Selective Oxidation of Methane into Formaldehyde and Carbon Monoxide Catalyzed by Supported Thermally Stable Iron Oxide Subnanoclusters Prepared from a Diiron-Introduced Polyoxometalate Precursor. *Appl. Catal. B - Environ.* **2022**, *314*, art. no. 121420.

(11) Tian J.; Tan J.; Zhang Z.; Han P.; Yin M.; Wan S.; Lin J.; Wang S.; Wang Y. Direct Conversion of Methane to Formaldehyde and CO on B_2O_3 Catalysts. *Nat. Commun.* **2020**, *11*, art. no. 5693.

(12) Jiang Y.; Li S.; Wang S.; Zhang Y.; Long C.; Xie J.; Fan X.; Zhao W.; Xu P.; Fan Y.; Cui C.; Tang Z. Enabling Specific Photocatalytic Methane Oxidation by Controlling Free Radical Type. *J. Am. Chem. Soc.* **2023**, *145*, 2698-2707.

(13) Mahlaba, S. V. L.; Hytoolakhan Lal Mahomed, N.; Govender, A.; Guo, J. F.; Leteba, G. M.; Cilliers, P. L.; van Steen, E. Platinum-Catalysed Selective Aerobic Oxidation of Methane to Formaldehyde in the Presence of Liquid Water. *Angew. Chem. Int. Ed.* **2022**, *61*, e202206841.

(14) Luo L.; Han X.; Wang K.; Xu Y.; Xiong L.; Ma J.; Guo Z.; Tang J. Nearly 100% Selective and Visible-Light-Driven Methane Conversion to Formaldehyde via Single-Atom Cu and $W^{\delta+}$. *Nat. Commun.* **2023**, *14*, art. no. 2690.

(15) Wang, Y.; Zhang, Y.; Wang, X.; Liu; Wu Z. Photothermal Direct Methane Conversion to Formaldehyde at the Gas-Solid Interface under Ambient Pressure. *Nat. Commun*. **2025**, *16*, art. no. 2550.

(16) Liu H. F.; Liu R. S.; Liew K. Y.; Johnson R. E.; Lunsford J. H. Partial Oxidation of Methane by Nitrous Oxide over Molybdenum on Silica. *J. Am. Chem. Soc.* **1984**, *106*, 4117-4121.

(17) Zhang X.; He D.; Zhang Q.; Xu B.; Zhu Q. Comparative Studies on Direct Conversion of Methane to Methanol/Formaldehyde over La−Co−O and ZrO_2 Supported Molybdenum Oxide Catalysts. *Top. Catal.* **2005**, *32*, 215-223.

(18) Fait M. J. G.; Ricci A.; Holena M.; Rabeah J.; Pohl M. M.; Linke D.; Kondratenko E. V. Understanding Trends in Methane Oxidation to Formaldehyde: Statistical Analysis of Literature Data and Based Hereon Experiments. *Catal. Sci. Technol.* **2019**, *9*, 5111-5121.

(19) Akiyama T.; Sei R.; Takenaka S. Partial Oxidation of Methane to Formaldehyde over Copper−Molybdenum Complex Oxide Catalysts. *Catal. Sci. Technol.* **2021**, *11*, 5273-5281.

(20) Meng X.; Cui X.; Rajan N. P.; Yu L.; Deng D.; Bao X. Direct Methane Conversion under Mild Condition by Thermo-, Electro-, or Photocatalysis. *Chem* **2019**, *5*, 2296-2325.

(21) Song H.; Meng X.; Wang S.; Zhou W.; Wang X.; Kako T.; Ye J. Direct and Selective Photocatalytic Oxidation of CH_4 to Oxygenates with O_2 on Cocatalysts/ZnO at Room Temperature in Water. *J. Am. Chem. Soc.* **2019**, *141*, 20507-20515.

(22) Li Y.; Wang M.; Ding Y. Q.; Zhao C. Y.; Ma J. B. Consecutive Methane Activation Mediated by Single Metal Boride Cluster Anions NbB_4^-. *Phys. Chem. Chem. Phys.* **2021**, *23*, 12592-12599.

(23) Schwarz H. Thermal Hydrogen-Atom Transfer from Methane: A Mechanistic Exercise. *Chem. Phys. Lett.* **2015**, *629*, 91-101.

(24) Li H. F.; Zhao Y. X.; Yuan Z.; Liu Q. Y.; Li Z. Y.; Li X. N.; Ning C. G.; He S. G. Methane Activation by Tantalum Carbide Cluster Anions $Ta_2C_4^-$. *J. Phys. Chem. Lett.* **2017**, *8*, 605-610.

(25) O'Hair R. A. J.; Khairallah G. N. Gas Phase Ion Chemistry of Transition Metal Clusters: Production, Reactivity, and Catalysis. *J. Clust. Sci.* **2004**, *15*, 331-363.

(26) Arutyunov V. S.; Strekova L. N. Gas Phase Ion Chemistry of Transition Metal Clusters: Production, Reactivity, and Catalysis. *J. Mol. Catal. A - Chem.* **2017**, *426*, 326-342.

(27) Ding X. L.; Wu X. N.; Zhao Y. X.; He S. G. C-H Bond Activation by Oxygen-Centered Radicals over Atomic Clusters. *Acc. Chem. Res.* **2012**, *45*, 382-390.

(28) Li Y. K.; Yuan Z.; Zhao Y. X.; Zhao C.; Liu Q. Y.; Chen H.; He S. G. Thermal Methane Conversion to Syngas Mediated by Rh_1-Doped Aluminum Oxide Cluster Cations $RhAl_3O_4^-$. *J. Am. Chem. Soc.* **2016**, *138*, 12854-12860.

(29) Schroder D.; Schwarz H. Gas-Phase Activation of Methane by Ligated Transition-Metal Cations. *Proc. Nat. Acad. Sci. U.S.A.* **2008**, 105, 18114-18119.

(30) Zhou S.; Li J.; Schlangen M.; Schwarz H. The Origin of the Efficient, Thermal Chemisorption of Methane by the Heteronuclear Metal-Oxide Cluster $[Al_2TaO_5]^+$. *Angew. Chem. Int. Ed.* **2016**, *55*, 14867-14871.

(31) Zhou S.; Li J.; Schlangen M.; Schwarz H. Spin-Selective Thermal Activation of Methane by Closed-Shell $[TaO_3]^+$. *Angew. Chem. Int. Ed.* **2016**, *55*, 7257-7260.

(32) Geng C.; Li J.; Weiske T.; Schwarz H. Thermal O–H Bond Activation of Water as Mediated by Heteronuclear $[Al_2Mg_2O_5]^{\bullet+}$: Evidence for Oxygen-Atom Scrambling. *J. Am. Chem. Soc.* **2018**, *140*, 9275-9281.

(33) Geng C.; Li J.; Weiske T.; Schwarz H. A Reaction-Induced Localization of Spin Density Enables Thermal C−H Bond Activation of Methane by Pristine FeC_4^+. *Chem. Eur. J.* **2019**, *25*, 12940-12945.
(34) Gupta S.; Kaur N.; Kumari I.; Goel N. Clusters as Catalysts: Advantages and Challenges. In *Chemical Modelling,* Vol/ 14, ed. M. Springborg and J. Joswig, The Royal Society of Chemistry, **2018**, 126-161.
(35) Schwarz H. Chemistry with Methane: Concepts Rather Than Recipes. *Angew. Chem. Int. Ed.* **2011**, *50*, 10096-10115.
(36) Schwarz H. How and Why Do Cluster Size, Charge State, and Ligands Affect the Course of Metal-Mediated Gas-Phase Activation of Methane? *Isr. J. Chem.* **2014**, *54*, 1413-1431.
(37) Schwarz, H.; Shaik, S.; Li, J., Electronic Effects on Room-Temperature, Gas-Phase C–H Bond Activations by Cluster Oxides and Metal Carbides: The Methane Challenge. *J. Am. Chem. Soc.* **2017**, *139*, 17201-17212.
(38) Lapoutre, V. J. F.; Redlich, B.; van der Meer, A. F. G.; Oomens, J.; Bakker, J. M.; Sweeney, A.; Mookherjee, A.; Armentrout, P. B. Structures of the Dehydrogenation Products of Methane Activation by 5d Transition Metal Cations. *J. Phys. Chem. A* **2013**, *117*, 4115−4126.
(39) Shayesteh, A.; Lavrov, V. V.; Koyanagi, G. K.; Bohme, D. K. Reactions of Atomic Cations with Methane: Gas Phase Room-Temperature Kinetics and Periodicities in Reactivity. *J. Phys. Chem. A* **2009**, *113*, 5602−5611.
(40) Lewis, T. W. R.; Viggiano, A. A.; Sweeny, B. C.; Meyer, J.; Ard, S. G.; Shuman, N. S. Mechanistic Foundations of the Sequential Activation of Methane by Ta^+: Oxidative Addition, Ring-Opening σ-Bond Metathesis, and C–C Bond Formation. *J. Phys. Chem. A* **2025**, 129, *19*, 4217-4233.
(41) Zhou, S. D.; Li, J. L.; Schlangen, M.; Schwarz, H. Bond Activation by Metal–Carbene Complexes in the Gas Phase. *Acc. Chem. Res.* **2016**, *49*, 494-502.
(42) Wang Z. C.; Dietl N.; Kretschmer R.; Ma J. B.; Weiske T.; Schlangen M.; Schwarz H. Direct Conversion of Methane into Formaldehyde Mediated by $[Al_2O_3]^+$ at Room Temperature. Angew. Chem., Int. Ed. 2012, 51, 3703-3707.
(43) Zhou S.; Schlangen M.; Schwarz H. Spin-Selective, Competitive Hydrogen-Atom Transfer versus CH_2O-Generation from the $CH_4/[ReO_4]^+$ Couple at Ambient Conditions. *Chem. Eur. J.* **2017**, *23*, 17469-17472.
(44) Wang L. N.; Zhou Z. X.; Li X. N.; Ma T. M.; He S. G. Thermal Conversion of Methane to Formaldehyde Promoted by Gold in $AuNbO_3^+$ Cluster Cations. *Chem. Eur. J.* **2015**, *21*, 6957-6961.
(45) Li Y. K.; Sun C. M.; Wei G. P.; He S. G.; Asmis K. R.; Zang S. Q. Thermal Methane Conversion to Formaldehyde Mediated by $NiAlO_3^+$ in the Gas Phase. *J. Phys. Chem. A* **2023**, *127*, 1636-1641.
(46) Li Z. Y.; Li H. F.; He S. G.; Zhao Y. X. Gold(III) Mediated Activation and Transformation of Methane on Au_1-Doped Vanadium Oxide Cluster Cations $AuV_2O_6^+$. *J. Am. Chem. Soc.* **2016**, *138*, 9437-9443.
(47) Yang Y.; Yang B.; He S. G.; Jiang L. X.; Li Z. Y.; Ren Y.; Xu H. G.; Zheng W. J.; Zhao Y. X. Direct Conversion of Methane with Carbon Dioxide Mediated by $RhVO_3^-$ Cluster Anions. *Angew. Chem., Int. Ed.* **2019**, *58*, 17287-17292.
(48) Zhao Y. X.; Li X. N.; Yuan Z.; Liu Q. Y.; Shi Q.; He S. G. Methane Activation by Gold-Doped Titanium Oxide Cluster Anions with Closed-Shell Electronic Structures. *Chem. Sci.* **2016**, *7*, 4730-4735.
(49) Zhao Y. X.; Li Z. Y.; Yuan Z.; Li X. N.; He S. G. Thermal Methane Conversion to Formaldehyde Promoted by Single Platinum Atoms in $PtAl_2O_4^-$ Cluster Anions. *Angew. Chem., Int. Ed.* **2014**, *53*, 9482-9486.
(50) Yuan Z.; Zhao Y. X.; Li X. N.; He S. G. Reactions of $V_4O_{10}^+$ Cluster Ions with Simple Inorganic and Organic Molecules. *Int. J. Mass Spectrom.* **2013**, *354-355*, 105-112.
(51) Wu X. N.; Xu B.; Meng J. H.; He S. G. C–H Bond Activation by Nanosized Scandium Oxide Clusters in Gas-Phase. *Int. J. Mass Spectrom.* **2012**, *310*, 57-64.
(52) Yuan Z.; Li Z. Y.; Zhou Z. X.; Liu Q. Y.; Zhao Y. X.; He S. G. Thermal Reactions of $(V_2O_5)_nO^-$ (n = 1–3) Cluster Anions with Ethylene and Propylene: Oxygen Atom Transfer versus Molecular Association. *J. Phys. Chem. C* **2014**, *118*, 14967-14976.
(53) Frisch M. J.; Trucks G. W.; Schlegel H. B.; Scuseria G. E.; Robb M. A.; Cheeseman J. R.; Scalmani G.; Barone V.; Petersson G. A.; Nakatsuji H.; Li X.; Caricato M.; Marenich A. V.; Bloino J.; Janesko B. G.; Gomperts R.; Mennucci B.; Hratchian H. P.; Ortiz J. V.; Izmaylov A. F.; Sonnenberg J. L.; Williams-Young D.; Ding F.; Lipparini F.; Egidi F.; Goings J.; Peng B.; Petrone A.; Henderson T.; Ranasinghe D.; Zakrzewski V. G.; Gao J.; Rega N.; Zheng G.; Liang W.; Hada M.; Ehara M.; Toyota K.; Fukuda R.; Hasegawa J.; Ishida M.; Nakajima T.; Honda Y.; Kitao O.; Nakai H.; Vreven T.; Throssell K.; Montgomery J. A., Jr.; Peralta J. E.; Ogliaro F.; Bearpark M. J.; Heyd J. J.; Brothers E. N.; Kudin K. N.; Staroverov V. N.; Keith T. A.; Kobayashi R.; Normand J.; Raghavachari K.; Rendell A. P.; Burant J. C.; Iyengar S. S.; Tomasi J.; Cossi M.; Millam J. M.; Klene M.; Adamo C.; Cammi R.; Ochterski J. W.; Martin R. L.; Morokuma K.; Farkas O.; Foresman J. B.; Fox D. J. *Gaussian 16,* Revision C.01; Gaussian, Inc.: Wallingford, CT, **2016**.
(54) Luo Y. R. Comprehensive Handbook of Chemical Bond Energies. CRC Press: Boca Raton, FL, **2007**.
(55) Yu H. S.; He X.; Truhlar D. G. MN15-L: A New Local Exchange-Correlation Functional for Kohn–Sham Density Functional Theory with Broad Accuracy for Atoms, Molecules, and Solids. *J. Chem. Theory Comput.* **2016**, *12*, 1280-1293.
(56) Andrae D.; Häußermann U.; Dolg M.; Stoll H.; Preuß H. Energy-Adjusted Ab Initio Pseudopotentials for the Second and Third Row Transition Elements. *Theor. Chim. Acta.* **1990**, *77*, 123-141.
(57) Dunning T. H. Gaussian Basis Sets for Use in Correlated Molecular Calculations. I. The Atoms Boron Through Neon and Hydrogen. *J. Chem. Phys.* **1989**, *90*, 1007-1023.
(58) Truhlar D.G.; Kuppermann A. Exact Tunneling Calculations. *J. Am. Chem. Soc.* **1971**, *93*, 1840-1851.
(59) Gonzalez C.; Schlegel H. B. An Improved Algorithm for Reaction Path Following. *J. Chem. Phys.* **1989**, *90*, 2154-2161.
(60) Gonzalez C.; Schlegel H. B. Reaction Path Following in Mass-Weighted Internal Coordinates. *J. Phys. Chem.* **1990**, *94*, 5523-5527.
(61) Pople J. A.; Gill P. M. W.; Handy N. C. Spin-Unrestricted Character of Kohn-Sham Orbitals for Open-Shell Systems. *Int. J. Quantum Chem.* **1995**, *56*, 303-305.
(62) Glendening E. D.; Landis C. R.; Weinhold F. NBO 6.0: Natural Bond Orbital Analysis Program. *J. Comput. Chem.* **2013**, 34, 1429-1437.
(63) Lu T.; Chen F. Multiwfn: A Multifunctional Wavefunction Analyzer. *J. Comput. Chem.* **2012**, *33*, 580-592.
(64) Kummerlöwe G.; Beyer M. K. Rate Estimates for Collisions of Ionic Clusters with Neutral Reactant Molecules. *Int. J. Mass Spectrom.* **2005**, *244*, 84–90.
(65) Gioumousis G.; Stevenson D. P. Reactions of Gaseous Molecule Ions with Gaseous Molecules. V. Theory. *J. Chem. Phys.* **1958**, *29*, 294–299.
(66) Harvey J. N. Spin-Forbidden Reactions: Computational Insight into Mechanisms and Kinetics. *WIREs. Comput. Mol. Sci*. **2013**, *4*, 1-14.
(67) Yang B.; Gagliardi L.; Truhlar D. G. Transition States of Spin-Forbidden Reactions. *Phys. Chem. Chem. Phys*. **2018**, *20*, 4129-4136.
(68) Shaik S. Two-State Reactivity: Personal Recounting of Its Conception and Future Prospects. *Isr. J. Chem*. **2020**, *60*, 938-956.
(69) Poli R.; Harvey J. N. Spin Forbidden Chemical Reactions of Transition Metal Compounds: New Ideas and New Computational Challenges. *Chem. Soc. Rev.* **2003**, *32*, 1-8.
(70) Mercero J. M.; Matxain J. M.; Lopez X.; York D. M.; Largo A.; Eriksson L. A.; Ugalde J. M. Theoretical Methods That Help Understanding the Structure and Reactivity of Gas Phase Ions. *Int. J. Mass Spectrom.* **2005**, *240,* 37-99.
(71) Steinfeld J. I.; Francisco J. S.; Hase W. L. *Chemical Kinetics and Dynamics*; Prentice-Hall: Hoboken, NJ, **1999**; p. 231.
(72) Steinfeld J. I.; Francisco J. S.; Hase W. L. *Chemical Kinetics and Dynamics*; Prentice-Hall: Upper Saddle River, NJ, **1999**; p. 313.
(73) Pavlov M.; Blomberg M. R. A.; Siegbahn P. E. M.; Wesendrup R.; Heinemann C.; Schwarz H. Pt^+-Catalyzed Oxidation of Methane: Theory and Experiment. *Phys. Chem. A* **1997**, 101, 1567−1579.
(74) Masubuchi T.; Eckhard J. F.; Goddard G.; Tschurl M.; Heiz U. Thermal C-O Coupling Reactions of Ta Methylene Clusters $[TanCH_2]^+$ (n=1, 4) with O_2. *Phys. Chem. Chem. Phys.* **2019**, *21*, 20743−20749.

(75) Yang Y.; Zhao Y. X.; He S. G. Conversion of CH_4 Catalyzed by Gas Phase Ions Containing Metals. *Chem. Eur. J.* **2022**, 28, art. no. e202200062.
(76) Shayesteh A.; Lavrov V. V.; Koyanagi G. K.; Bohme D. K. Reactions of Atomic Cations with Methane: Gas Phase Room-Temperature Kinetics and Periodicities in Reactivity. *J. Phys. Chem. A* **2009**, *113*, 5602–5611.
(77) Ruscic. B.; Bross, D. H. Active Thermochemical Tables (ATcT) values based on ver. 1.220 of the Thermochemical Network, Argonne National Laboratory, Lemont, Illinois, USA (2025); available at ATcT.anl.gov [DOI: 10.17038/CSE/2568691] (accessed Dec. 22, 2025)
(78) Fukui K.; Inagaki S. Orbital Interaction Rationale for the Role of Catalysts. *J. Am. Chem. Soc.* **1975***, 97*, 445-4452.

Table of Contents artwork

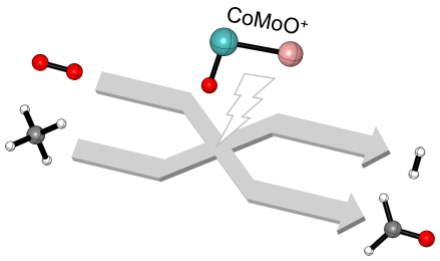

$CH_4 + 1/2O_2 \rightarrow H_2 + HCHO$